Discs of mammalian rod photoreceptors form through the membrane evagination mechanism

Jin-Dong Ding,[1] Raquel Y. Salinas,[2] and Vadim Y. Arshavsky[1,2]

[1]Department of Ophthalmology and [2]Department of Pharmacology and Cancer Biology, Duke University Medical Center, Durham, NC 27710

Photoreceptor discs are membrane organelles harboring components of the visual signal transduction pathway. The mechanism by which discs form remains enigmatic and is the subject of a major controversy. Classical studies suggest that discs are formed as serial plasma membrane evaginations, whereas a recent alternative postulates that discs, at least in mammalian rods, are formed through intracellular vesicular fusion. We evaluated these models in mouse rods using methods that distinguish between the intracellular vesicular structures and plasma membrane folds independently of their appearance in electron micrographs. The first differentiated membranes exposed to the extracellular space from intracellular membranes; the second interrogated the orientation of protein molecules in new discs. Both approaches revealed that new discs are plasma membrane evaginations. We further demonstrated that vesiculation and plasma membrane enclosure at the site of new disc formation are artifacts of tissue fixation. These data indicate that all vertebrate photoreceptors use the evolutionary conserved membrane evagination mechanism to build their discs.

Introduction

The light-sensing outer segment compartment of vertebrate photoreceptor cells is a striking example of how the anatomical organization of a cellular organelle well suits its function. Outer segments are cylindrical or conical structures filled with hundreds to a few thousand flattened membrane organelles, called photoreceptor discs. Discs undergo continuous renewal throughout the animal's lifespan, with new membranes added at the outer segment base and old membranes shed at the tip (Young, 1967). Disc stacks provide multiple membrane layers densely packed with visual pigment molecules, which ensures highly efficient light capture. Conceptually, this structural organization is similar to that of thylakoids in chloroplasts, which likewise evolved to maximize light absorption. Disc membranes also comprise vast surfaces for lateral protein diffusion, a process required to amplify the signal downstream of photoexcited visual pigment (Arshavsky and Burns, 2014). Signal amplification is particularly critical for dim-light vision performed by rod photoreceptors because it allows them to produce sizable electrical responses to stimuli as small as single photons (Baylor et al., 1979).

The structural organization of outer segments differs between rods and cones (Kennedy and Malicki, 2009; Pearring et al., 2013). Rod outer segments contain "closed discs," which are physically and electrically separate from the surrounding plasma membrane and possess distinct protein and lipid compositions. In contrast, cones, which are evolutionarily older than rods, possess "open discs" that are contiguous infoldings of the plasma membrane. A hybrid arrangement has also been documented for mammalian cones, in which some discs are open and others are closed (Anderson et al., 1978; Bunt, 1978; Carter-Dawson and LaVail, 1979).

Separation of discs from the plasma membrane aids rods in functioning as single photon detectors because it provides cytosolic space for second messenger diffusion along the inner surface of the plasma membrane, thereby engaging many channels in generating an electrical response to light. What is not understood is how discs are formed. The classic hypothesis postulates that new discs in all photoreceptor types are formed from outgrowths (evaginations) of the plasma membrane at the outer segment base; these evaginations are exposed to the extracellular space and appear on electron micrographs as open discs (Laties et al., 1976; Kinney and Fisher, 1978; Steinberg et al., 1980). A key characteristic differentiating rods from cones is that, once the evaginating membrane reaches its final diameter, it fuses at the edge with the outer segment plasma membrane to form an enclosed disc.

The concept that new discs form as plasma membrane evaginations arose from the studies of lower vertebrates using membrane-associating fluorescent dyes, which label plasma membrane but do not penetrate inside the cells to label intracellular membrane structures (Laties et al., 1976; Matsumoto and Besharse, 1985). These dyes intensely label membranes of newly formed but not mature discs in rods, demonstrating that new discs are open to the extracellular environment, whereas unlabeled mature discs are shielded by the outer segment plasma membrane. Unfortunately, attempts to apply this

Correspondence to Vadim Y. Arshavsky: vadim.arshavsky@duke.edu

Abbreviation used in this paper: GA, glutaraldehyde.

The Rockefeller University Press $30.00
J. Cell Biol. Vol. 211 No. 3 495–502
www.jcb.org/cgi/doi/10.1083/jcb.201508093

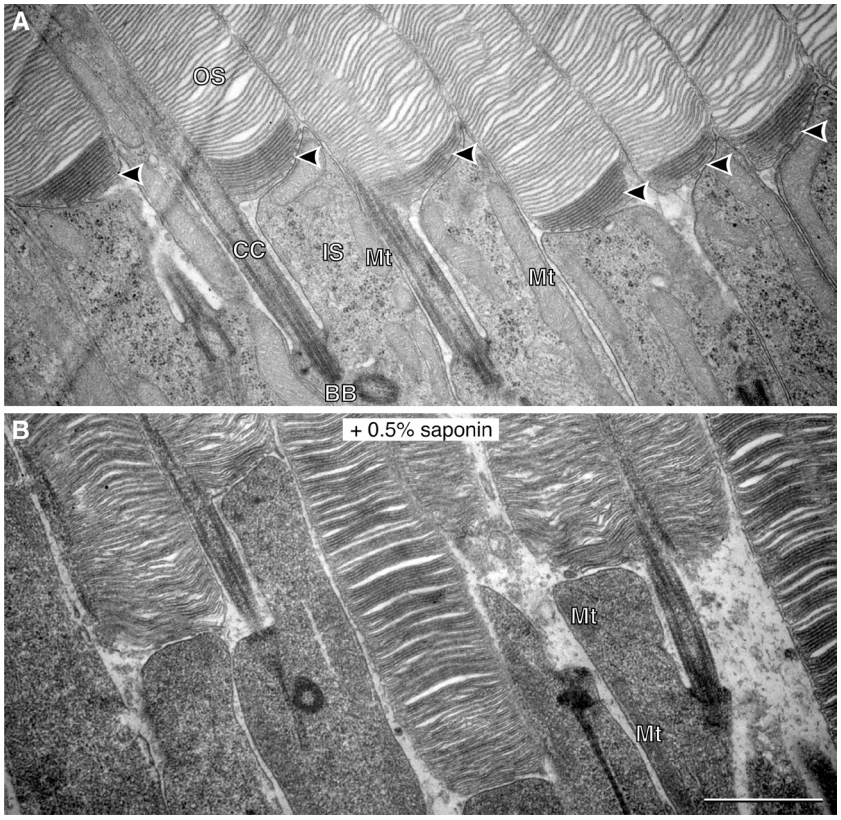

Figure 1. **New discs at the rod outer segment base are accessible to tannic acid.** (A) EM image of a mouse retina section at the interface between rod outer and inner segments stained with tannic acid–uranyl acetate. Arrowheads point at densely stained, tightly packed new discs at the outer segment base; note that mature discs are less densely stained and slightly swollen. (B) Permeabilization of the plasma membrane with 0.5% saponin results in equal density staining of new and mature discs by tannic acid–uranyl acetate. BB, basal body; CC, connecting cilium; IS, inner segment; Mt, mitochondria; OS, outer segment. Bar, 1 µm.

technique to elucidate whether new discs are open in mammalian rods have not succeeded (Laties et al., 1976).

The alternative, more recent hypothesis of disc morphogenesis in rods (Chuang et al., 2007) suggests that discs are formed upon vesicular fusion at the outer segment base. This hypothesis gained significant traction in subsequent years because many EM studies of mammalian rods showed outer segments completely enclosed by the plasma membrane, often with vesicular material at the outer segment base (Chuang et al., 2007, 2015; Lobanova et al., 2008; Gilliam et al., 2012; Chakraborty et al., 2014); see also earlier studies (Miyaguchi and Hashimoto, 1992; Obata and Usukura, 1992). On the other hand, other EM studies reported that the base of mouse rod outer segments contains several open discs (Carter-Dawson and LaVail, 1979; Arikawa et al., 1992; Patil et al., 2012). It was argued that the outer segment base contains proteins known to perform vesicular fusion, most notably syntaxin 3 (Chuang et al., 2007). However, the presence of fusion proteins at the outer segment base is compatible with both models because each postulates distinct membrane fusion events. Because the rest of the evidence for each mechanism is derived from observations of electron micrographs, supporters of each hypothesis suggested that the discrepancy in new disc appearance is explained by technical artifacts of tissue fixation (Kennedy and Malicki, 2009; Pearring et al., 2013). But which of the two appearances reflects rod outer segment structure in vivo?

In this study, we answered this question by using two novel methods that test key predictions of each model without relying on the appearance of new discs on EM. The first differentiated membranes exposed to the extracellular space from intracellular membranes, whereas the second interrogated the orientation of rhodopsin molecules in new discs. Both approaches provided clear evidence that new discs in mouse rods are formed as membrane evaginations. Lastly, we compared various protocols of tissue preparation for ultrastructural analysis and concluded that both plasma membrane enclosure and membrane vesiculation at the rod outer segment base originate from delayed fixation of the retina. Collectively, our data support the membrane evagination hypothesis and indicate that rods of all vertebrate species use the single, evolutionary conserved membrane evagination mechanism for disc morphogenesis.

Results and discussion

Newly formed rod discs are open to the extracellular space

To investigate the ultrastructure of newly formed discs in mammalian rods, we developed a method that provides superior preservation of the outer retina and preferentially stains membranes exposed to the extracellular space. Two critical elements of this method are immediate in vivo perfusion of mice with fixative and treatment of retinal tissue with the tannic acid–uranyl acetate membrane contrasting reagent. Much like membrane-impermeable fluorescent dyes, tannic acid poorly penetrates intact membranes, yielding intense plasma membrane staining and lesser staining of intracellular membrane structures (Fedorko and Levine, 1976; Núnez-Durán, 1980). Therefore, the presence of any open discs would be revealed by their intense staining in electron micrographs.

Images of the mouse retina processed by this technique show that each rod outer segment contains several discs at its base, which appear open and are more intensely stained than mature discs that are closed (Fig. 1 A). This differential accessibility to tannic acid demonstrates that membranes of new discs are directly exposed to the extracellular space, whereas mature

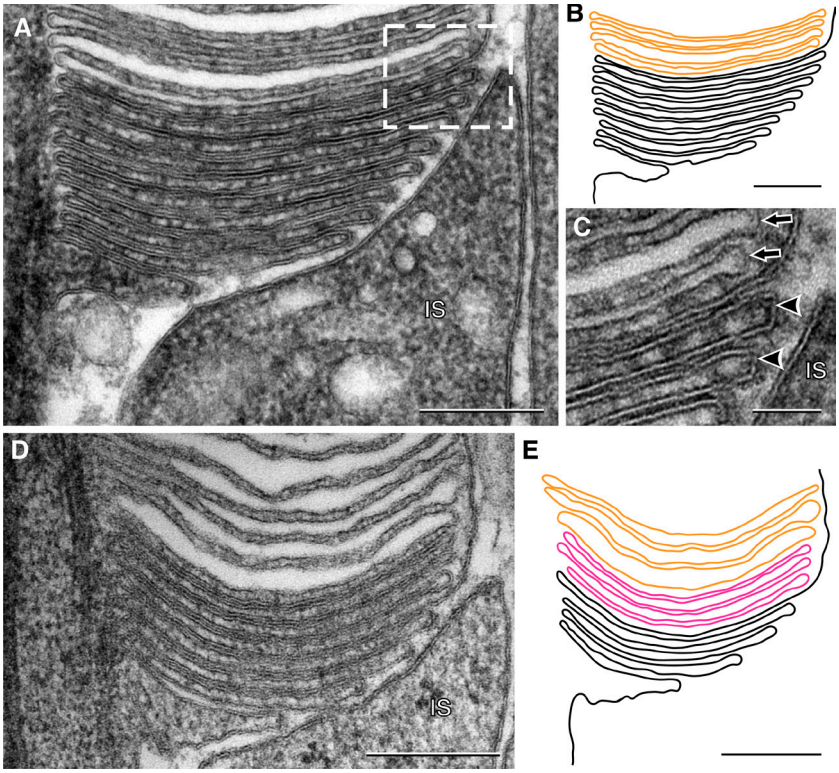

Figure 2. **New discs form as plasma membrane evaginations.** (A and D) Representative magnified images of the rod outer segment base. (B and E) Traces of the plasma membrane folds from the images in panels A and D. Open discs are black, mature discs are orange, and discs that are enclosed in this section plane but still highly accessible to tannic acid are magenta. (C) Magnified view of the area boxed in A. Arrowheads point to triple-layered membranes of new discs, and arrows point to mature discs that do not display this pattern. Bars: (A–E) 200 nm; (C) 50 nm. IS, inner segment.

discs are shielded by the plasma membrane enclosing the rest of the outer segment. Another difference between newly formed and mature discs is that the latter appear slightly swollen, which likely reflects their reaction to osmotic conditions of tissue preparation documented previously (Heller et al., 1971; Korenbrot et al., 1973). In contrast, new discs do not swell, consistent with their openness to the extracellular space.

In a control experiment, we permeabilized membranes in the retinal tissue with 0.5% saponin, which allows tannic acid to penetrate into the intracellular space. We predicted that the difference between staining of new and mature discs would diminish. In fact, saponin treatment resulted in uniform staining of all outer segment membranes, with no difference between new and mature discs (Fig. 1 B). Saponin also increased the overall density of intracellular membrane structures, such as mitochondria within rod inner segments, further highlighting the unique property of tannic acid to differentiate between exposed and protected membranes.

New discs in rods form as contiguous plasma membrane evaginations

Another benefit of our method is the exceptional preservation of new disc ultrastructure (Fig. 2 A). This allowed to closely follow each fold of the plasma membrane in the region of new disc formation, from the connecting cilium to the fusion point, as illustrated in Fig. 2 B. Thorough examination of more than 200 individual rods, in which the location of outer segment base can be clearly identified, revealed that the number of densely stained discs ranged from 6 to 12, and none of these cells contained vesicular structures in this region.

Another signature characteristic of membranes exposed to extracellular space is their classical triple-layered staining pattern, with two darker layers outside and a lighter layer inside (Robertson, 1981). Intracellular membranes, including membranes of mature discs, lack this pattern, probably because of their limited access to tannic acid. This is particularly easy to appreciate in the higher-magnification view (Fig. 2 C).

Interestingly, many rods contained one to five discs, which appeared enclosed but still exhibited dense triple-layer membrane staining with no evidence of swelling (Fig. 2, D and E). This could be explained by these discs undergoing the process of enclosure when the fixative was applied, so they were partially open to the extracellular space, although at a region outside the plane of a given section.

An additional observation in Fig. 3 (A and B) is that the bendings of the membrane at the two opposite edges of new discs are differently shaped: "hairpin"-like at the axoneme side and less curved "paperclip"-like at the opposite side. However, once the fusion is completed, mature discs acquire the hairpin-like shape on both sides (similar observations were made for monkey rods [Steinberg et al., 1980]). It was previously shown that the hairpin-like membrane bend can be induced by peripherin (Kevany et al., 2013), a protein whose oligomers support the disc rim structure (Goldberg, 2006). Therefore, we directly tested whether a given shape of the disc edge correlates with the presence of peripherin.

We examined peripherin localization at both types of disc edges using immunogold labeling (Fig. 3, C–F) and found that the mean number of gold particles detected at the hairpin-shaped edges of new discs was ∼19-fold larger than at the paperclip-like edges (Fig. 3 G). This striking difference suggests that disc enclosure is concomitant with fortification of its edge by peripherin oligomers. Our observation is consistent with an early study by Arikawa et al. (1992), who showed lower density of peripherin labeling in the same region of rod outer segments in rats. However, we also determined that the mean number of gold particles at the axonemal edge of new discs was ∼1.7-fold larger than at the edges of mature discs above, further suggesting that peripherin is first concentrated at

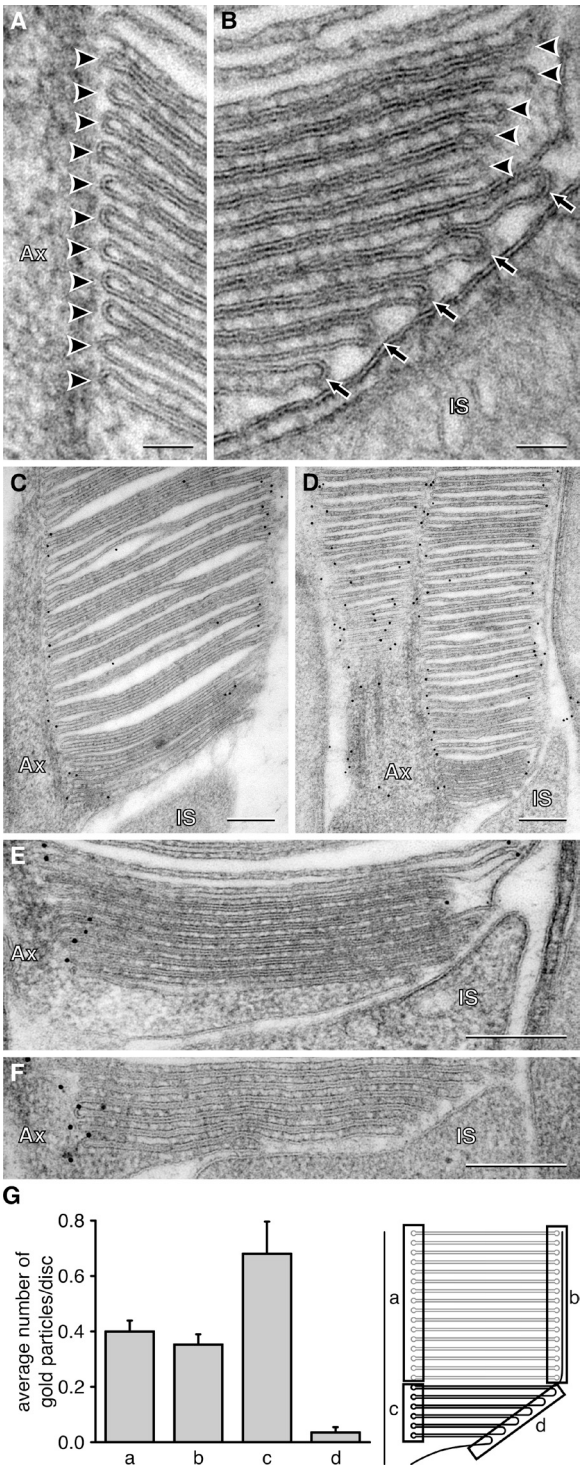

Figure 3. **Different shape and peripherin content at opposing edges of new discs.** (A) Edges of new discs at the axonemal side of the outer segment base. (B) Edges of new discs at the side opposite to the axoneme. (C) and (D) Examples of two rod outer segments immunogold-labeled for peripherin. (E) and (F) High magnification images of two rod outer segment bases immunogold-labeled for peripherin. (G) The mean number of gold particles per disc measured in four regions illustrated in the cartoon to the right. Particles within 100 nm from the discs edges were counted. The data are averaged from 15 rods; error bars represent SEM. The P value for the difference between c and d is 7.2×10^{-6} and between a and c is 0.04 from a Student's *t* test. Arrowheads point to the hairpin-shaped disc edges; arrows point to paperclip-like disc edges. Bars: (A and B) 50 nm; (C–F) 200 nm. Ax, axoneme; IS, inner segment.

this location and then redistributes evenly along the disc edge upon membrane enclosure.

Rhodopsin membrane topology supports the evagination model of disc morphogenesis

A major distinction between the membrane evagination and vesicular fusion hypotheses lies in the orientation of rhodopsin molecules in the newly formed discs. The evagination hypothesis postulates that new discs have rhodopsin's N terminus exposed to the extracellular space. However, when the disc edge fuses with plasma membrane, a topological inversion of the membrane occurs, resulting in rhodopsin's N terminus facing inside the disc lumen and C terminus exposed outside. In contrast, the vesicular fusion hypothesis postulates that rhodopsin's N terminus faces the disc lumen in both new and mature discs because intracellular vesicular fusion is not accompanied by membrane inversion.

To investigate the membrane orientation of rhodopsin in new discs, we performed postembedment immunogold labeling of rhodopsin using antibodies specifically recognizing its N or C terminus: 4D2 and 1D4, respectively (Fig. 4, A–D). We counted the number of gold particles located immediately outside the edges of new discs, as illustrated in Fig. 4 E. After normalizing these counts by the total number of gold particles within the entire area of new discs, we found that the prevalence of particles produced by N-terminal antibody labeling was ∼2.2-fold higher than that by C-terminal antibody labeling. This shows that rhodopsin in new discs faces the extracellular space with its N terminus (Fig. 4 F), an orientation consistent with the model of membrane evagination but not vesicular fusion. (The presence of gold particles representing rhodopsin's C terminus outside new discs is expected, given that gold particles in this technique could be found at distances of up to ∼20 nm from the epitope [Amiry-Moghaddam and Ottersen, 2013], whereas the membrane thickness is only ∼7 nm.)

Plasma membrane enclosure and disc vesiculation are postmortem artifacts of tissue fixation

Finally, we aimed to identify the origin of membrane vesiculation and enclosure at the rod outer segment base, reported in the references cited earlier. Previous EM studies of other tissues (Hasty and Hay, 1978; Tao-Cheng et al., 2007; Ding et al., 2013) showed that cellular ultrastructure, particularly in neurons, can rapidly change after an animal's death. This process could be further facilitated by delayed fixation, such as perfusing an animal with saline before administering the fixative (Chuang et al., 2007). Using their protocol, we completely replaced blood with heparin saline before perfusing mice with our standard paraformaldehyde/glutaraldehyde fixative or the paraformaldehyde/acrolein used in the study by Chuang et al. (2007) (Fig. 5, A–G). This modification resulted in an appreciable fraction of rods containing vesicular structures at the outer segment base (quantified in Fig. 5 I) and/or plasma membrane enclosure. Interestingly, in our study, new discs in most rods fixed with paraformaldehyde/acrolein were still open, in contrast to the study by Chuang et al. (2007). This result highlights how unstable these structures are and emphasizes that our protocol provides unsurpassed structural preservation of the extremely fragile rod outer segment base (notably, the study by Steinberg et al. [1980] directly perfused fixative with no saline flush as well).

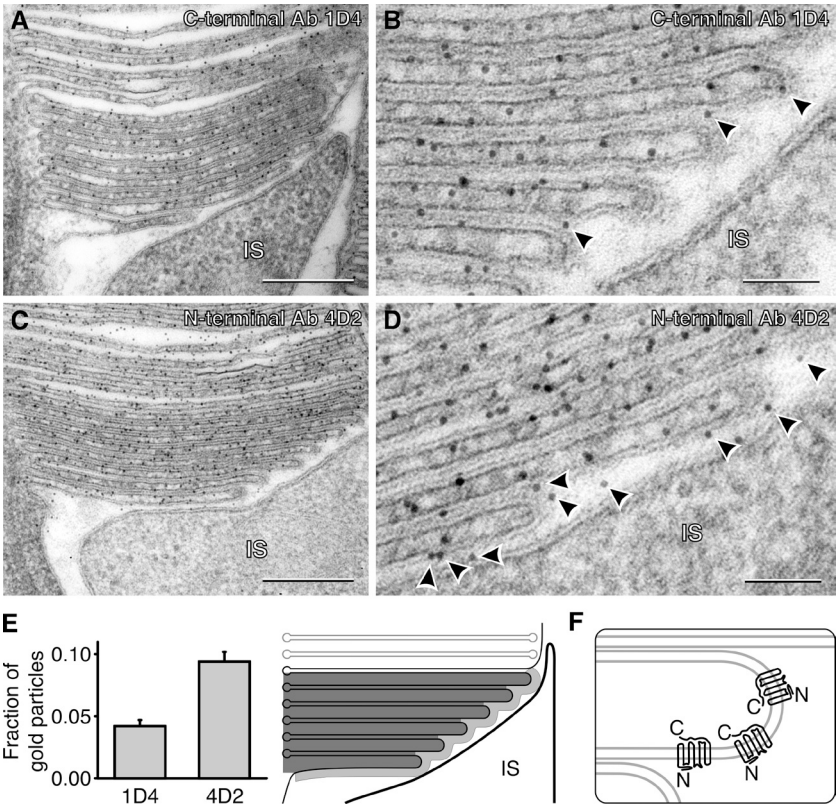

Figure 4. **Rhodopsin topology in the membranes of newly formed discs.** (A and B) Low- and high-magnification images of rhodopsin immunogold labeling by the 1D4 antibody recognizing the C terminus of rhodopsin. (C and D) Low- and high-magnification images of rhodopsin immunogold labeling by the 4D2 antibody recognizing the N terminus of rhodopsin. (E) Relative abundance of gold particles in the extracellular space adjacent to the membranes of newly formed discs. The number of particles produced by rhodopsin immunogold labeling by each antibody was counted within a 30-nm region of the extracellular space between membranes of new discs and the inner-segment plasma membrane. This region is depicted by light gray in the cartoon on the right and particles used in the count are marked by arrowheads in B and D. These counts were normalized by the total number of gold particles counted in the region of newly formed open discs of the same cell (marked by dark gray in the cartoon to the right from the graph). The number of analyzed cells labeled by each antibody was 13; error bars represent SEM; P = 0.0009. (F) Cartoon representation of rhodopsin orientation in the membrane of newly formed discs. Bars: (A and C) 200 nm; (B and D) 50 nm. IS, inner segment.

To further test the sensitivity of disc structure to fixation methods, we replicated several common procedures used in retinal EM studies. First, we immersed eyecups into fixative (Lobanova et al., 2008; Chakraborty et al., 2014) and found distorted outer segment morphology in most rods (Fig. 5 G). This distortion affected all cells when paraformaldehyde, much more rapidly penetrating into tissues than glutaraldehyde, was omitted from the fixative (Fig. 5, H and I). We also replaced glutaraldehyde in our original protocol with acrolein (Chuang et al., 2007) but did not perfuse the animal with saline. In this case, new discs remained open and highly accessible to tannic acid, confirming that structural artifacts produced in their study are caused by delayed fixation and not the use of acrolein as the fixative. However, the overall morphology of new discs fell short of that obtained with paraformaldehyde/glutaraldehyde fixation (Fig. S1, A and B). Finally, we replaced tannic acid with the conventionally used osmium tetroxide (Fig. S1, C and D). Although new discs had an open appearance, the preservation of their structure, once again, fell short of that obtained with tannic acid.

Collectively, these data demonstrate that evaginating membranes of new discs are extremely unstable and prone to fuse or vesiculate in postmortem retinas. However, once discs are enclosed and their edges assume the hairpin shape fortified by peripherin, they stabilize and do not easily vesiculate. Such a thermodynamic instability of new discs is likely to explain why a recent cryo-electron tomography study of isolated mouse rod outer/inner segment preparations reported new discs enclosed by plasma membrane (Gilliam et al., 2012). Before cryofixation, these preparations underwent rounds of vortexing and centrifugation, which provided ample opportunities for new discs to fuse before being frozen (notably, the authors mentioned that some cells displayed open discs at the outer segment base).

In summary, our findings support the evagination model of disc morphogenesis and explain that evidence supporting the vesicular fusion hypothesis represent artifacts of tissue fixation. Combined with classical observations by Steinberg et al. (1980) and other studies cited in the preceding paragraphs, they indicate that mammalian rods and cones form their discs through the universal plasma membrane evagination mechanism. Although elucidating the molecular details of this process is the challenge of future investigations, our results provide a clear conceptual framework for exploring this fascinating biological process.

Materials and methods

Animal perfusion and tissue fixation

Animal studies were conducted in compliance with the US Department of Health and Human Services Guide for the Care and Use of Laboratory Animals and were approved by the Institutional Animal Care and Use Committee of Duke University. In our standard protocol, C57Bl6/J mice (4–12 wk old; The Jackson Laboratory) were deeply anesthetized with ketamine/xylazine (100/10 mg/kg) and immediately transcardially perfused for 10 min with 15 ml fixative containing 2% paraformaldehyde, 2% glutaraldehyde, and 0.05% $CaCl_2$ in 50 mM MOPS buffer, pH 7.4. Their enucleated eyes were postfixed in the same fixative for 1 h. A modification of this protocol included mouse perfusion with 10 ml heparin (1,000 U/ml) saline before paraformaldehyde/glutaraldehyde administration. Alternatively, we used the protocol used in the study by Chuang et al. (2007). In brief, mice were sequentially perfused with 10 ml heparin saline administered for 2 min, 20 ml 4% paraformaldehyde/3.75% acrolein (Polysciences) in 0.1 M sodium phosphate buffer, pH 7.4, and finally 60 ml of 4% paraformaldehyde in 0.1 M sodium phosphate buffer. Enucleated eyes were postfixed in 2% glutaraldehyde in 0.1 M sodium phosphate

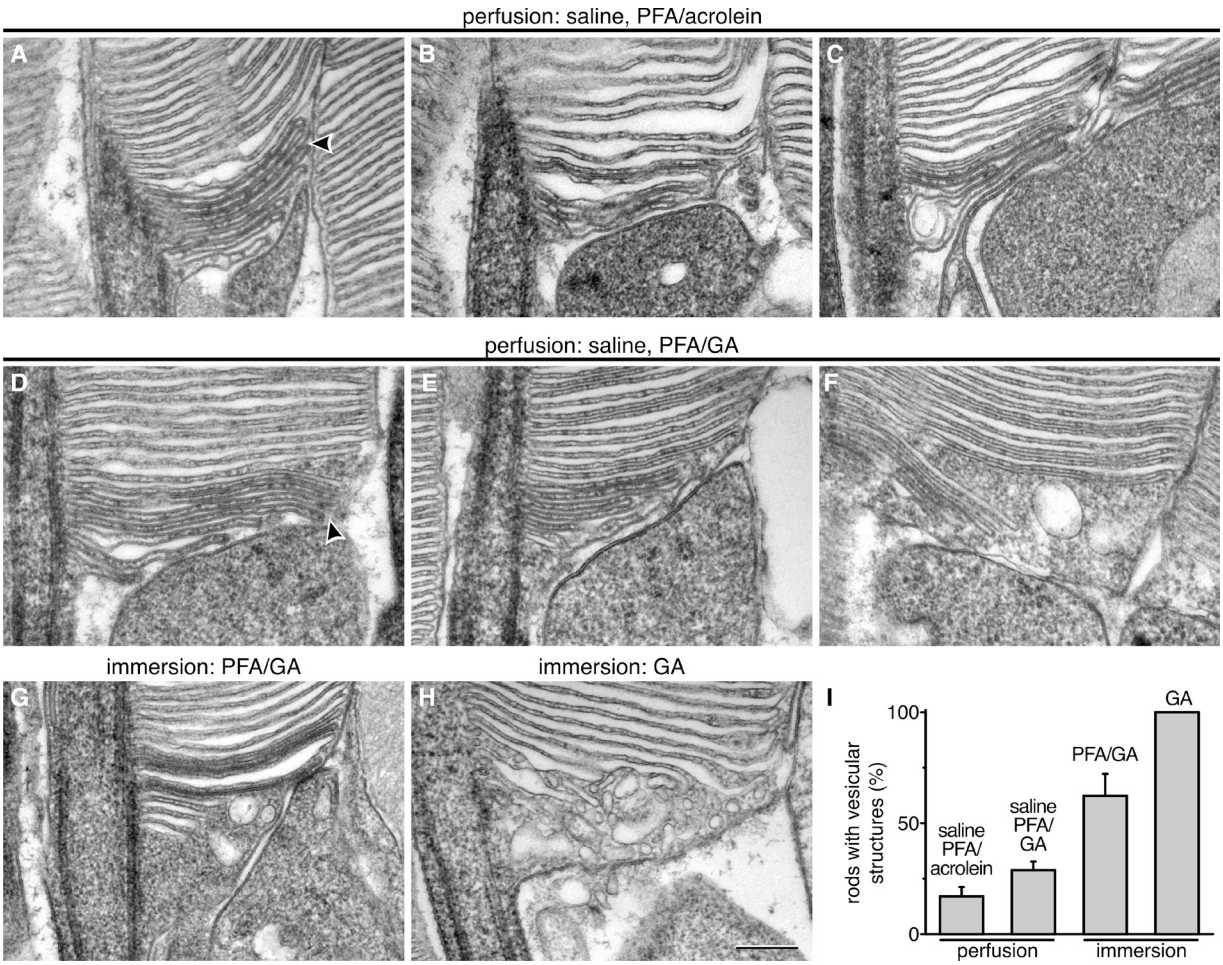

Figure 5. **Perturbations of rod outer segment structure caused by variations in tissue preparation procedure.** (A–C) Representative EM images of rod outer segment bases fixed according to Chuang et al. (2007) and treated with tannic acid–uranyl acetate. (D–F) Representative EM images of rod outer segment bases obtained after introducing an additional heparin saline perfusion step before paraformaldehyde/glutaraldehyde (PFA/GA) fixation. (G and H) Representative EM image of a rod outer segment base obtained from eyecups immersed in PFA/GA (G) or GA (H) fixative. (I) Quantification of the fraction of rods containing vesicular structures at the outer segment base. The number of cells analyzed for each condition was 138 (saline PFA/acrolein), 343 (saline PFA/GA), 57 (PFA/GA), and 31 (GA). The data are averaged from cell counts in three mice treated under each condition; error bars represent SEM. Arrowheads point to the membrane fusion points. Bar, 200 nm. See also Fig. S1.

buffer, pH 7.4, for 1 h. A modification of this protocol included direct mouse perfusion with fixative, omitting the saline step. Upon the completion of animal perfusion, eyeballs were rinsed with PBS, cornea and lens were removed, the posterior eye cups were embedded in 5% agar (A1296; Sigma-Aldrich), and cut on a vibratome (Leica) at 100–200-µm sections.

A subset of experiments was performed with immersion-fixed eyecups. Mice were euthanized with CO_2 and decapitated. Eyes were enucleated and eyecups immersed in 2% paraformaldehyde, 2% glutaraldehyde, and 0.05% $CaCl_2$ in 50 mM MOPS buffer, pH 7.4, or 2% glutaraldehyde and 0.05% $CaCl_2$ in 50 mM MOPS buffer for 1 h. Posterior eye cups were then embedded and sectioned as described in the preceding paragraph.

Tissue processing for transmission EM

The tannic acid–uranyl acetate tissue processing protocol was slightly modified from Phend et al. (1995). In brief, vibratome sections were treated with 1% tannic acid (Electron Microscopy Sciences) in 0.1 M Hepes, pH 7.4, for 1 h. Sections were rinsed with 0.1 M maleate buffer, pH 6.0, and then treated with 1% uranyl acetate (Electron Microscopy Sciences) in the same buffer for 1 h. Sections were rinsed, dehydrated with ethanol, infiltrated, and embedded with Spurr low-viscosity resin between two sheets of ACLAR films (Electron Microscopy Sciences). To test the effect of membrane permeability on the staining pattern of tannic acid–uranyl acetate, 0.5% saponin (Sigma-Aldrich) was added to the tannic acid solution.

A subset of samples was processed using the osmium tetroxide method as in Ding et al. (2015). Vibratome sections were treated with 1% osmium tetroxide in 0.1 M phosphate buffer for 1 h, mordanted en bloc with 1% uranyl acetate, dehydrated, and embedded in Spurr resin.

60–80-nm ultrathin sections were cut with an ultramicrotome (Leica), collected on copper grids (Electron Microscopy Sciences), and poststained with 1% uranyl acetate and Sato's lead (Sato, 1968).

Postembedment immunogold labeling

Sections for postembedment immunogold labeling were prepared as in Ding et al. (2013) with minor modifications. In brief, vibratome sections were treated with 0.5% tannic acid and cryoprotected with 30% glycerol in 0.1 M sodium acetate. Sections were freeze-substituted overnight in 4% uranyl acetate/95% methanol at −78°C while being gently shaken on dry ice. Sections were then rinsed with methanol, infiltrated with Lowicryl HM-20 (Electron Microscopy

Sciences), slowly warmed to 0°C, and embedded for 3 d under ultraviolet light. Ultrathin sections were cut at 60–80 nm and collected on nickel grids coated with a grid-coating pen (Daido Sangyo). Grids were treated in 10 mM citric buffer, pH 6.0, containing 0.005% Tergitol NP-10 for 15 min at 60°C, rinsed with water, blocked with 1% glycine in Tris-buffered saline, pH 7.6, containing 0.005% Tergitol NP-10 for 30 min, and incubated overnight with primary antibodies: (a) rabbit anti-peripherin, residues 296–346 (1:5,000; provided by G.H. Travis, University of California, Los Angeles, Los Angeles, CA; Kedzierski et al., 1999); (b) mouse anti-rhodopsin C terminus (1:5,000; 1D4; Abcam); and (c) mouse anti-rhodopsin N terminus (1:5,000; 4D2; Abcam). Grids were rinsed with buffer, blocked with 1% donkey serum, and probed with donkey anti–mouse or anti–rabbit IgG conjugated to 6- or 12-nm colloidal gold (1:50; Jackson ImmunoResearch Laboratories, Inc.) for 2 h. Grids were rinsed and counterstained with uranyl acetate and Sato's lead.

Image acquisition and data analysis

Samples were examined using a JEM-1400 electron microscope (JEOL) at 60 kV. Images were collected using an Orius CCD camera (Gatan) and DigitalMicrograph software, version 1.71.38 (Gatan). Brightness, contrast, and curves were adjusted to the entire images using Adobe Photoshop, version CS4. Distances between features on electron micrographs were measured using ImageJ, version 1.50a (National Institutes of Health). The number of animals analyzed for each condition varied between two (Fig. 5, G and H) and five (Figs. 1 and 2).

For the analysis of peripherin immunogold labeling, we counted gold particles within the arbitrarily chosen 100-nm distance from the disc edges. For the analysis of rhodopsin immunogold labeling in new discs, we counted the number of gold particles within 30 nm of the extracellular space between the membrane border of new discs and the inner segment plasma membrane. The resulting value was normalized by the total number of gold particles found in the area representing open, newly formed discs of the same cell. The 30-nm restriction was based on the maximal estimated distance between the membrane surface and the gold particle, considering that neither terminus of rhodopsin extends further than ∼10 nm from the membrane, the size of each primary and secondary antibody does not exceed ∼8 nm (Amiry-Moghaddam and Ottersen, 2013), and the radius of the gold particle is 3 nm.

Online supplemental material

Fig. S1 shows perturbations of rod outer segment structure caused by acrolein or osmium tetroxide. Online supplemental material is available at http://www.jcb.org/cgi/content/full/jcb.201508093/DC1.

Acknowledgments

We thank the Duke Eye Center Morphology/Image Processing Core facility for assistance in using the electron microscope.

This work was supported by National Institutes of Health grants EY022862 (R.Y. Salinas), EY12859 (V.Y. Arshavsky), and EY5722 (V.Y. Arshavsky) and by an unrestricted grant and Nelson Trust Award (V.Y. Arshavsky) from Research to Prevent Blindness.

The authors declare no competing financial interests.

Submitted: 24 August 2015
Accepted: 25 September 2015

References

Amiry-Moghaddam, M., and O.P. Ottersen. 2013. Immunogold cytochemistry in neuroscience. *Nat. Neurosci.* 16:798–804. http://dx.doi.org/10.1038/nn.3418

Anderson, D.H., S.K. Fisher, and R.H. Steinberg. 1978. Mammalian cones: Disc shedding, phagocytosis, and renewal. *Invest. Ophthalmol. Vis. Sci.* 17:117–133.

Arikawa, K., L.L. Molday, R.S. Molday, and D.S. Williams. 1992. Localization of peripherin/rds in the disk membranes of cone and rod photoreceptors: Relationship to disk membrane morphogenesis and retinal degeneration. *J. Cell Biol.* 116:659–667. http://dx.doi.org/10.1083/jcb.116.3.659

Arshavsky, V.Y., and M.E. Burns. 2014. Current understanding of signal amplification in phototransduction. *Cell. Logist.* 4:e29390. http://dx.doi.org/10.4161/cl.29390

Baylor, D.A., T.D. Lamb, and K.W. Yau. 1979. Responses of retinal rods to single photons. *J. Physiol.* 288:613–634.

Bunt, A.H. 1978. Fine structure and radioautography of rabbit photoreceptor cells. *Invest. Ophthalmol. Vis. Sci.* 17:90–104.

Carter-Dawson, L.D., and M.M. LaVail. 1979. Rods and cones in the mouse retina. I. Structural analysis using light and electron microscopy. *J. Comp. Neurol.* 188:245–262. http://dx.doi.org/10.1002/cne.901880204

Chakraborty, D., S.M. Conley, M.R. Al-Ubaidi, and M.I. Naash. 2014. Initiation of rod outer segment disc formation requires RDS. *PLoS One.* 9:e98939. http://dx.doi.org/10.1371/journal.pone.0098939

Chuang, J.Z., Y. Zhao, and C.H. Sung. 2007. SARA-regulated vesicular targeting underlies formation of the light-sensing organelle in mammalian rods. *Cell.* 130:535–547. http://dx.doi.org/10.1016/j.cell.2007.06.030

Chuang, J.Z., Y.C. Hsu, and C.H. Sung. 2015. Ultrastructural visualization of trans-ciliary rhodopsin cargoes in mammalian rods. *Cilia.* 4:4. http://dx.doi.org/10.1186/s13630-015-0013-1

Ding, J.D., M.B. Kennedy, and R.J. Weinberg. 2013. Subcellular organization of camkii in rat hippocampal pyramidal neurons. *J. Comp. Neurol.* 521:3570–3583. http://dx.doi.org/10.1002/cne.23372

Ding, J.D., U. Kelly, M. Landowski, C.B. Toomey, M. Groelle, C. Miller, S.G. Smith, M. Klingeborn, T. Singhapricha, H. Jiang, et al. 2015. Expression of human complement factor H prevents age-related macular degeneration-like retina damage and kidney abnormalities in aged Cfh knockout mice. *Am. J. Pathol.* 185:29–42. http://dx.doi.org/10.1016/j.ajpath.2014.08.026

Fedorko, M.E., and R.F. Levine. 1976. Tannic acid effect on membrane of cell surface origin in guinea pig megakaryocytes and platelets. *J. Histochem. Cytochem.* 24:601–605. http://dx.doi.org/10.1177/24.4.58024

Gilliam, J.C., J.T. Chang, I.M. Sandoval, Y. Zhang, T. Li, S.J. Pittler, W. Chiu, and T.G. Wensel. 2012. Three-dimensional architecture of the rod sensory cilium and its disruption in retinal neurodegeneration. *Cell.* 151:1029–1041. http://dx.doi.org/10.1016/j.cell.2012.10.038

Goldberg, A.F. 2006. Role of peripherin/rds in vertebrate photoreceptor architecture and inherited retinal degenerations. *Int. Rev. Cytol.* 253:131–175. http://dx.doi.org/10.1016/S0074-7696(06)53004-9

Hasty, D.L., and E.D. Hay. 1978. Freeze-fracture studies of the developing cell surface. II. Particle-free membrane blisters on glutaraldehyde-fixed corneal fibroblasts are artefacts. *J. Cell Biol.* 78:756–768. http://dx.doi.org/10.1083/jcb.78.3.756

Heller, J., T.J. Ostwald, and D. Bok. 1971. The osmotic behavior of rod photoreceptor outer segment discs. *J. Cell Biol.* 48:633–649. http://dx.doi.org/10.1083/jcb.48.3.633

Kedzierski, W., J. Weng, and G.H. Travis. 1999. Analysis of the rds/peripherin.rom1 complex in transgenic photoreceptors that express a chimeric protein. *J. Biol. Chem.* 274:29181–29187. http://dx.doi.org/10.1074/jbc.274.41.29181

Kennedy, B., and J. Malicki. 2009. What drives cell morphogenesis: A look inside the vertebrate photoreceptor. *Dev. Dyn.* 238:2115–2138. http://dx.doi.org/10.1002/dvdy.22010

Kevany, B.M., Y. Tsybovsky, I.D. Campuzano, P.D. Schnier, A. Engel, and K. Palczewski. 2013. Structural and functional analysis of the native peripherin-ROM1 complex isolated from photoreceptor cells. *J. Biol. Chem.* 288:36272–36284. http://dx.doi.org/10.1074/jbc.M113.520700

Kinney, M.S., and S.K. Fisher. 1978. The photoreceptors and pigment epithelium of the larval Xenopus retina: Morphogenesis and outer segment renewal. *Proc. R. Soc. Lond. B Biol. Sci.* 201:149–167. http://dx.doi.org/10.1098/rspb.1978.0037

Korenbrot, J.I., D.T. Brown, and R.A. Cone. 1973. Membrane characteristics and osmotic behavior of isolated rod outer segments. *J. Cell Biol.* 56:389–398. http://dx.doi.org/10.1083/jcb.56.2.389

Laties, A.M., D. Bok, and P. Liebman. 1976. Procion yellow: A marker dye for outer segment disc patency and for rod renewal. *Exp. Eye Res.* 23:139–148. http://dx.doi.org/10.1016/0014-4835(76)90197-4

Lobanova, E.S., S. Finkelstein, R. Herrmann, Y.M. Chen, C. Kessler, N.A. Michaud, L.H. Trieu, K.J. Strissel, M.E. Burns, and V.Y. Arshavsky. 2008. Transducin γ-subunit sets expression levels of α- and β-subunits and is crucial for rod viability. *J. Neurosci.* 28:3510–3520. http://dx.doi.org/10.1523/JNEUROSCI.0338-08.2008

Matsumoto, B., and J.C. Besharse. 1985. Light and temperature modulated staining of the rod outer segment distal tips with Lucifer yellow. *Invest. Ophthalmol. Vis. Sci.* 26:628–635.

Miyaguchi, K., and P.H. Hashimoto. 1992. Evidence for the transport of opsin in the connecting cilium and basal rod outer segment in rat retina: Rapid-freeze, deep-etch and horseradish peroxidase labelling studies. *J. Neurocytol.* 21:449–457. http://dx.doi.org/10.1007/BF01191508

Núnez-Durán, H. 1980. Tannic acid as an electron microscope tracer for permeable cell membranes. *Stain Technol.* 55:361–365.

Obata, S., and J. Usukura. 1992. Morphogenesis of the photoreceptor outer segment during postnatal development in the mouse (BALB/c) retina. *Cell Tissue Res.* 269:39–48. http://dx.doi.org/10.1007/BF00384724

Patil, H., N. Tserentsoodol, A. Saha, Y. Hao, M. Webb, and P.A. Ferreira. 2012. Selective loss of RPGRIP1-dependent ciliary targeting of NPHP4, RPGR and SDCCAG8 underlies the degeneration of photoreceptor neurons. *Cell Death Dis.* 3:e355. http://dx.doi.org/10.1038/cddis.2012.96

Pearring, J.N., R.Y. Salinas, S.A. Baker, and V.Y. Arshavsky. 2013. Protein sorting, targeting and trafficking in photoreceptor cells. *Prog. Retin. Eye Res.* 36:24–51. http://dx.doi.org/10.1016/j.preteyeres.2013.03.002

Phend, K.D., A. Rustioni, and R.J. Weinberg. 1995. An osmium-free method of epon embedment that preserves both ultrastructure and antigenicity for post-embedding immunocytochemistry. *J. Histochem. Cytochem.* 43:283–292. http://dx.doi.org/10.1177/43.3.7532656

Robertson, J.D. 1981. Membrane structure. *J. Cell Biol.* 91:189s–204s. http://dx.doi.org/10.1083/jcb.91.3.189s

Sato, T. 1968. A modified method for lead staining of thin sections. *J. Electron Microsc. (Tokyo).* 17:158–159.

Steinberg, R.H., S.K. Fisher, and D.H. Anderson. 1980. Disc morphogenesis in vertebrate photoreceptors. *J. Comp. Neurol.* 190:501–508. http://dx.doi.org/10.1002/cne.901900307

Tao-Cheng, J.H., P.E. Gallant, M.W. Brightman, A. Dosemeci, and T.S. Reese. 2007. Structural changes at synapses after delayed perfusion fixation in different regions of the mouse brain. *J. Comp. Neurol.* 501:731–740. http://dx.doi.org/10.1002/cne.21276

Young, R.W. 1967. The renewal of photoreceptor cell outer segments. *J. Cell Biol.* 33:61–72. http://dx.doi.org/10.1083/jcb.33.1.61